Curvature and dynamical spacetimes: can we peer into the quantum regime?

OPEN ACCESS
IOP Publishing
Classical and Quantum Gravity
Class. Quantum Grav. **40** (2023) 065008 (14pp)
https://doi.org/10.1088/1361-6382/acb9cd

Curvature and dynamical spacetimes: can we peer into the quantum regime?

Vitor Cardoso[1,2], **David Hilditch**[2], **Krinio Marouda**[2,*], **José Natário**[3] **and Ulrich Sperhake**[4]

[1] Niels Bohr International Academy, Niels Bohr Institute, Blegdamsvej 17, 2100 Copenhagen, Denmark
[2] CENTRA, Departamento de Física, Instituto Superior Técnico—IST, Universidade de Lisboa—UL, Avenida Rovisco Pais 1, 1049-001 Lisboa, Portugal
[3] CAMGSD, Departamento de Matemática, Instituto Superior Técnico—IST, Universidade de Lisboa—UL, Avenida Rovisco Pais 1, 1049-001 Lisboa, Portugal
[4] Department of Applied Mathematics and Theoretical Physics, Centre for Mathematical Sciences, University of Cambridge, Wilberforce Road, Cambridge CB3 0WA, United Kingdom

E-mail: krinio.marouda@tecnico.ulisboa.pt

Received 30 September 2022; revised 27 January 2023
Accepted for publication 7 February 2023
Published 23 February 2023

Abstract

Stationary compact astrophysical objects such as black holes and neutron stars behave as classical systems from the gravitational point of view. Their (observable) curvature is everywhere 'small'. Here we investigate whether mergers of such objects, or other strongly dynamical spacetimes such as collapsing configurations, may probe the strong-curvature regime of general relativity. Our results indicate that dynamical black hole spacetimes always result in a modest increase $\sim$3 in the Kretschmann scalar, relative to the stationary state. In contrast, we find that the Kretschmann scalar can dynamically increase by orders of magnitude, during the gravitational collapse of scalar fields, and that the (normalized) peak curvature does *not* correspond to that of the critical solution. Nevertheless, without fine tuning of initial data, this increase lies far below that needed to render quantum-gravity corrections important.

* Author to whom any correspondence should be addressed.

Keywords: curvature in dynamical spacetimes, gravitational collapse, 1-loop corrections to GR

(Some figures may appear in colour only in the online journal)

1. Introduction

The advent of gravitational-wave (GW) astronomy [1, 2] and of very long baseline interferometry [3, 4] opened exciting new windows to the invisible Universe. Compact objects, in particular neutron stars and black holes (BHs), play a unique role in the endeavor to test our understanding of general relativity (GR) and in the search for new physics [5–11].

According to the singularity theorems [12, 13], classical GR must fail in BH interiors. Quantum mechanics in BH spacetimes also leads to puzzling consequences, such as the information paradox [14–16]. It is tempting to conjecture that a theory of quantum gravity will resolve these issues, but the scale and nature of quantum gravity corrections to BH spacetimes is unknown.

In this paper we ask a simple but outlandish question: can dynamical, astrophysical processes probe the quantum gravity regime?

The inclusion of backreaction of quantum fluctuations is a delicate problem in General Relativity [17]. Working at semi-classical level, the renormalized 1-loop effective action admits a low-curvature expansion of the form [17–19]

$$S_{\rm eff}=\int d^4x\sqrt{-g}\left(-\Lambda_{\rm eff}+\frac{R}{16\pi G_{\rm eff}}+\mathcal{L}^{(1)}_{\rm eff}+\dots\right), \tag{1}$$

$$\mathcal{L}^{(1)}_{\rm eff}={M_{\rm P}}^2\left(a_1R^2+a_2R_{\alpha\beta}R^{\alpha\beta}+a_3R_{\alpha\beta\gamma\delta}R^{\alpha\beta\gamma\delta}\right), \tag{2}$$

where $\Lambda_{\rm eff}\,, G_{\rm eff}$ are the effective cosmological and Newton's constant, respectively, and $M_{\rm P}$ is the Planck mass (we work with geometric units $c=1={G_{\rm eff}}$ throughout). The precise values of the constants a_i are not necessary for us here, but they can be calculated exactly in a semi-classical framework. The important aspect is that higher-curvature terms are expected to be present generically; variants of this argument come from effective field theory approaches. The most general theory without new degrees of freedom, compatible with observations, and obeying some basic principles, can be shown to be Einstein's theory corrected by higher-order derivative terms [17–20].

The above provides a general framework to look for quantum gravitational effects. Setups for which the Kretschmann or other higher-derivative invariants are too large are not described by small corrections to the classical theory: one is then in the quantum regime. A similar motivation is behind recent studies of quantum gravitational anomalies and their impact on photons from coalescences of compact objects [21, 22], or studies of gravity with higher-order corrections [23].

Unfortunately, the (lowest-order) corrections relative to the classical equations of motion are expected to scale as $(M_{\rm P}/M)^2\sim 10^{-76}$ or smaller, with M the mass of the macroscopic object under study (say, a neutron star or stellar mass BH). For *equilibrium* compact configurations, these quantum corrections are indeed small: consider a neutron star of mass M and radius $r\sim 6M$; the Kretschmann scalar—equation (3)—is $K_1\lesssim 0.1M^{-4}$, whereas the Ricci scalar at the surface is $R\sim M/r^3=0.04M^{-2}$. Thus, in such an equilibrium scenario, higher order curvature corrections are expected to be around 76 orders of magnitude smaller than the classical terms.

In the absence of the ultimate theory of quantum gravity, we ask the following question: can higher curvature terms *ever* become important during a *dynamical* evolution? Take a neutron

star collapsing to a non-spinning BH: we know that the BH interior harbours strong-curvature regions; is it possible that outward propagating photons or gravitons had access to 'unnaturally large' curvature regions? This question is related, but not identical, to claims on cosmic censorship violations [24]. In other words, we are not so much concerned with curvatures reaching arbitrarily large values but rather with how much larger than their stationary values they can become during a generic dynamical evolution (and in particular whether they can become Planckian).

2. Quantities of interest

There are five quadratic invariants constructed from the Riemann and the Weyl tensors [25] (there are also cubic invariants, but we will not consider them here): the Kretschmann invariant, the Chern–Pontryagin invariant, the Euler invariant, and the first and second Weyl invariants. Three of these can be computed from the others once the energy momentum tensor is known. Therefore, we focus solely on two invariants, the Kretschmann scalar

$$K_1 \equiv R_{\alpha\beta\gamma\delta}R^{\alpha\beta\gamma\delta}\,, \tag{3}$$

and the Chern–Pontryagin invariant

$$K_2 \equiv {}^\star RR = \frac{1}{2}R_{\alpha\beta\gamma\delta}\epsilon^{\alpha\beta\mu\nu}R^{\gamma\delta}{}_{\mu\nu}\,. \tag{4}$$

Note that K_2 is necessarily zero for spherically symmetric spacetimes, as the antipodal map is an orientation-reversing isometry.

3. Oppenheimer–Snyder collapse

Arguably, the simplest model of a gravitational collapse is that of Oppenheimer–Snyder, where a ball of dust with uniform density collapses to a Schwarzschild BH. The metric inside the dust ball can therefore be written as

$$ds^2 = -d\tau^2 + a^2(\tau)(d\rho^2 + \rho^2 d\Omega^2)\,, \tag{5}$$

where $d\Omega^2$ is the line element of the unit 2-sphere and we assumed, for simplicity, the metric to be spatially flat. The metric outside the dust ball is, of course, the Schwarzschild metric

$$ds^2 = -\left(1-\frac{2M}{r}\right)dt^2 + \left(1-\frac{2M}{r}\right)^{-1}dr^2 + r^2 d\Omega^2\,, \tag{6}$$

where M is the mass of the final BH. At the boundary of the dust ball we have [26]

$$\mu = \frac{3M}{4\pi r^3}\,, \tag{7}$$

where μ is the ball's density. As the Weyl tensor vanishes inside the dust ball, $K_1 = \frac{5}{3}(8\pi\mu)^2$, corresponding to

$$K_1 = \frac{60M^2}{r^6} \tag{8}$$

at the ball's boundary. Since the Kretschmann invariant K_1 is constant along constant τ hypersurfaces, and increasing with τ, the events in the dust ball with largest K_1 visible from the

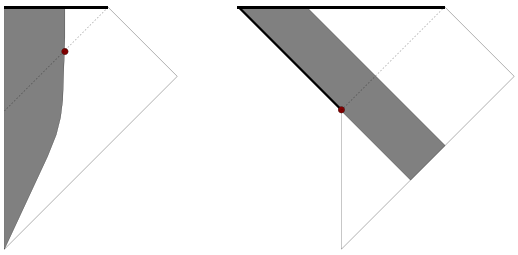

Figure 1. Penrose diagrams for the Oppenheimer–Snyder and the critical null dust collapses. The shaded regions correspond to the dust, the dashed lines to the event horizons, and the thick lines to the singularities. The red dots mark the points where the Kretschmann invariant K_1 is maximal along the horizon (infinite in the case of the critical Vaidya solution).

exterior correspond to the intersection of the dust ball's boundary with the event horizon (see figure 1), where

$$K_1 = \frac{15}{16M^4}\,. \tag{9}$$

This is slightly larger (by a factor of $5/4$) than the maximum value observable in the Schwarzschild exterior, where

$$K_1 = \frac{48M^2}{r^6} < \frac{3}{4M^4}\,. \tag{10}$$

It is interesting to note that the nature of the curvature inside and outside the dust ball is completely different: whereas inside the Weyl tensor vanishes and there is only Ricci curvature, outside it is the Ricci tensor that vanishes, leaving only the Weyl curvature.

It is possible to obtain much larger values of the Kretschmann scalar by considering inhomogeneous dust collapses. In fact, it is well known that such collapses can even produce naked singularities, corresponding to shell crossings or shell focusing [27, 28]. If one is careful to cover these singularities with the event horizon [29], arbitrarily large (but finite) values of K_1 can be observed from the exterior; however, this requires fine-tuning, and such collapses are quite dissimilar to realistic astrophysical collapses. A straightforward example of this can be seen in the limiting case of null dust collapses, which we now briefly discuss.

4. Null radiation collapse

Another simple model of collapse can be obtained form the Vaidya metric [30], given by

$$ds^2 = -\left(1 - \frac{2M(v)}{r}\right) dv^2 + 2dvdr + r^2 d\Omega^2, \tag{11}$$

where $M(v)$ is an arbitrary function of the advanced time v. This metric corresponds to the energy-momentum tensor

$$T = \frac{1}{4\pi r^2}\frac{dM}{dv} dv \otimes dv\,, \tag{12}$$

describing a null dust propagating along the incoming radial null geodesics. Choosing $M(v)$ to vary from 0 to some final value M_1 on some interval $v \in [0, v_1]$, and constant outside this interval, provides a simple model of BH formation, as the metric coincides with the Minkowski metric for $v < 0$ and with the Schwarzschild metric of mass M_1 for $v > v_1$. The Kretschmann scalar is still given by equation (10), and so we see that we can obtain arbitrarily large curvatures outside the event horizon if $M(v) > 0$ near $r = 0$. It turns out that by fine-tuning the free function $M(v)$ it is possible to arrange for the Penrose diagram of the Vaydia solution to be as depicted in figure 1 [31–34] (as an example, if $M(v)$ is taken to be of the form $M(v) = \mu v$ for $v \in [0, v_1]$ then the fine-tuning amounts to choosing $8M_1/v_1 = 1 + \sqrt{1-\mu^2}$). This diagram represents a critical solution, separating naked singularities from BHs; for these solutions, the event horizon emanates from the first singularity, and so K_1 attains arbitrarily large values on the event horizon (in the example above, $K_1 = C/v^4$ along the event horizon, where $C = C(\mu)$ is a positive constant). Small perturbations of these solutions lead to BHs whose event horizons no longer emanate from the first singularity, and so we can have arbitrarily large (but finite) values of K_1 visible from the exterior. However, these perturbations are very particular solutions, quite distant from any conceivable astrophysical scenario. They would correspond to initial data either already displaying large curvatures, or carefully fine-tuned to produce them via focusing.

5. Massless minimally coupled scalar field collapse

Another classical setup of collapse in spherical symmetry is the numerical study of BH formation due to a self-gravitating scalar field minimally coupled to gravity. We will use this as a proxy for gravitational collapse of stars to BHs in astrophysical setups. We use horizon-penetrating coordinates, namely Kerr–Schild coordinates, which allow probing the formation of the apparent horizon and also to study the behaviour of the curvature invariants throughout the whole evolution, before and after the horizon forms. The metric is constructed using ingoing and outgoing null vectors and their associated covectors:

$$\xi = \partial_t + C_+ \partial_r\,, \quad \underline{\xi} = \partial_t + C_- \partial_r\,,$$

$$\eta = -C_+ dt + dr\,, \quad \underline{\eta} = C_- dt - dr\,.$$

Here, C_+ and C_- control the local behaviour of the lightcones in these coordinates. Due to spherical symmetry, all the evolved variables in this section are functions of (t, r) only. The spherically symmetric ansatz for the metric using these null covectors is the following:

$$ds^2 = -\frac{e^\delta}{C_+ - C_-}\left(\eta \otimes \underline{\eta} + \underline{\eta} \otimes \eta\right) + r^2 d\Omega^2\,, \tag{13}$$

where δ is associated to the determinant of the metric in the (t, r) plane. We will be using the Kerr–Schild gauge [35] with r areal radius and $C_- = -1$, and work with the renormalized variable

$$\tilde{C}_+ = \frac{2C_+}{C_+ + 1}\,. \tag{14}$$

In other words, the ingoing characteristic speed has been set to $C_- = -1$ everywhere in spacetime, while the radial coordinate has been taken to be the areal radius.

The field equations with a stress energy tensor of a massless minimally coupled scalar field ψ in the matter sector reduce to two evolution equations

$$\nabla_{\underline{\xi}}\delta = -4\pi r T_{\underline{\xi}\underline{\xi}}\,, \tag{15}$$

$$\nabla_{\underline{\xi}}\left(re^{-\delta}\tilde{C}_{+}\right) = 4\pi r^2 e^{-\delta}T_{\underline{\xi\xi}} - 1\,, \tag{16}$$

and one constraint equation

$$\frac{\partial_r\left(re^{-\delta}\tilde{C}_{+}\right)-1}{\tilde{C}_{+}-2} = 2\pi r^2 e^{-\delta}\left(\tilde{C}_{+}T_{\underline{\xi\xi}} - (\tilde{C}_{+}-2)T_{\xi\xi}\right)\,. \tag{17}$$

We solve these field equations for the variables $\tilde{C}_{+}, \delta$ together with the wave equation for the scalar field, $\Box_g\psi = 0$, written as a first order system on the variables $\Pi = \partial_t\psi$ and $\Phi = \partial_r\psi$. We use a Runge–Kutta with method of lines, second order finite differencing, and Kreiss–Oliger dissipation.

The ADM mass in these coordinates is computed as

$$M_{\rm ADM} = \lim_{R\to\infty}\left[r\left(1 - \frac{e^{-\frac{\delta}{2}}}{\sqrt{2-\tilde{C}_{+}}}\right)\right]\,, \tag{18}$$

and is independent of t throughout the evolution, since the spacelike slices capture both the strong field region and the scalar radiation. The horizon mass is given by

$$M_{\rm AH} = \sqrt{\frac{A_{\rm AH}}{16\pi}}\,, \tag{19}$$

where $A_{\rm AH}$ is the area of the apparent horizon. Throughout we will discuss results obtained via apparent horizon properties. We have calculated also the event horizon location dynamically in a subset of cases, and find that our conclusions are not affected qualitatively.

We choose the scalar field in the initial $(t=0)$ slice to be a localised Gaussian of amplitude P and standard deviation σ centered at $r = r_0$,

$$\psi(0,r) = \frac{P}{\sqrt{2\pi\sigma}}\left(e^{-\left(\frac{r-r_0}{\sigma}\right)^2} + e^{-\left(\frac{r+r_0}{\sigma}\right)^2}\right)\,, \tag{20}$$

while all the other free functions are set to zero, and solve for $\tilde{C}_{+}(0,r)$ using the constraint equation (17). There is no BH in our initial slice because using the above initial profiles for the grid functions and assuming regularity at the origin, $\tilde{C}_{+}(0,0) = 1$, the equation admits a solution of the form

$$\tilde{C}_{+}(0,r) = \frac{1}{r}e^{-4\pi\int_0^r \tilde{r}\Phi(0,\tilde{r})^2 d\tilde{r}}\left[1 + e^{4\pi\int_0^\zeta \tilde{r}\Phi(0,\tilde{r})^2 d\tilde{r}}\right] > 0\,,$$

where ζ is an integration constant. For sufficiently large initial amplitude, however, an apparent horizon forms during the evolution, which in these coordinates simply corresponds to the condition $\tilde{C}_{+} = 0$. In fact, the expansion of the congruence of radial outgoing null geodesics is computed as

$$\Theta = \frac{2C_{+}}{r} \tag{21}$$

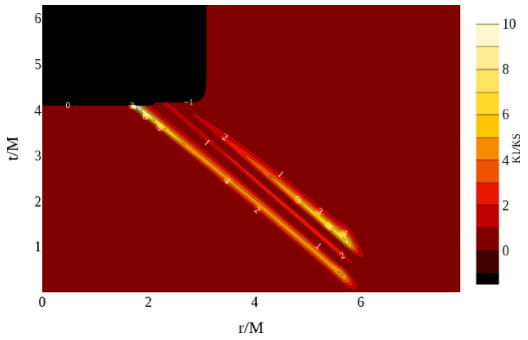

Figure 2. Contour of the Kretschmann invariant K_1 in the (t, r) plane, in units of the relevant invariant K_S in equation (22), of a static Schwarzschild with mass equal to the mass of the apparent horizon of a newly formed BH, $M_{\rm AH} = 3.17$. The invariant K_1 grows during the evolution, with the maximum happening close to the initial location of the apparent horizon.

in these coordinates. After an apparent horizon forms, we perform BH excision a few time steps later, and keep on evolving the domain of outer communications.

To understand how the dynamics drives the curvature invariants, we normalize our results by the Kretschmann scalar of the newly formed BH, i.e. expression (10) evaluated at the apparent horizon,

$$K_{\rm S} = \frac{3}{4M_{\rm AH}^4}\,. \tag{22}$$

In this way, we avoid getting large curvature invariants as an artifact of 'small' initial conditions that led to a small BH: we are interested in astrophysical setups, and therefore would like to learn if large gradients are possible even when the final object is a stellar-mass BH.

Our results are summarized in figures 2–4.[5] After the apparent horizon forms, the peak of K_1 occurs close to the AH/EH for 'small' amplitude of initial data, while for 'stronger' data the maximum can also be located away from the horizon, since there is an outgoing pulse of scalar radiation.

For the range of initial data that we have studied here, we observe that $K_{\rm max}/K_{\rm S}$ is always $\lesssim 10^3$ (see figure 3). This is a much greater increase than in the analytic example of homogeneous dust collapse discussed above. We find that for some configurations the maximum curvature K_1 may arise from early time evolution of data which itself has a large curvature. Although we suspect that this problem can be circumvented by prescribing initial data 'further in the past,' we decided to be conservative and normalize our results to K_1/A, with $A = \max\left(K_{\rm max}|_{t=0}, K_S\right)$. The results are shown in figure 4.

For a fixed radius r_0 and width σ, we find that the curvature K_1 peaks at a finite value of the amplitude P, as depicted in figure 4. Our results are well described by

$$\frac{\max K_1}{A} = \alpha\left(\frac{r_0}{\sigma}\right)^{\gamma}\,, \tag{23}$$

for small σ, where $\alpha = 33 \pm 3$ and $\gamma = 0.6 \pm 0.1$.

[5] We note that [36] also studied the spherically symmetric collapse of a (massive) scalar field, but focused on the behaviour of K along a timelike curve approaching the singularity.

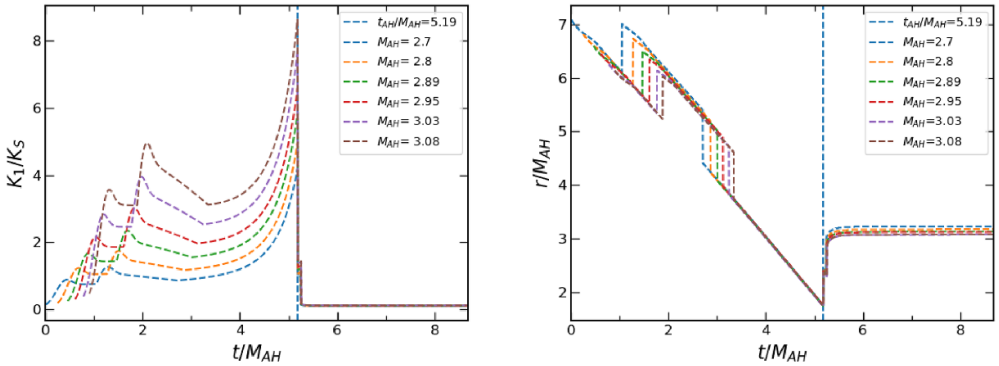

Figure 3. Left Panel: evolution of the maximum of the Kretschmann invariant K_1 normalized by K_S (see equation (22)). All the plots have been shifted in time so that the apparent horizon formation occurs at $t_{\rm AH} = 5.2M_{\rm AH}$. The initial pulse is centered at $R_0 = 20$, with $\sigma = 2$. Right Panel: location of the maximum of K_1 during the same evolution. Note that the location of the maximum jumps in the beginning because some other local maximum takes over as the global maximum. However, close to the time of the apparent horizon formation, the global maximum is at some radius smaller than the radius of the apparent horizon that forms later.

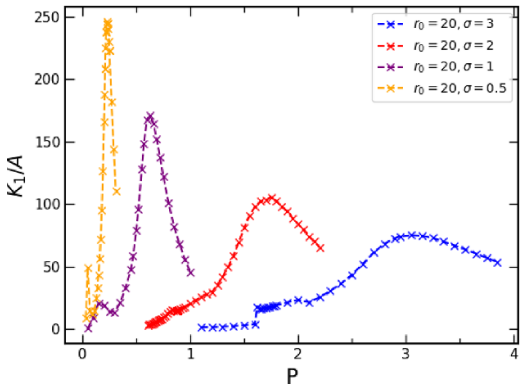

Figure 4. Global maximum of K_1 for the scalar field collapse, in units of $A = \max\left(K_{\max}|_{t=0}, K_S\right)$, shown for four series of evolutions of pulses centered at $r_0 = 20$, with width $\sigma = 0.5, 1, 2, 3$, respectively, and varying P. The discontinuity observed for $\sigma = 3$ is due to the outgoing scalar pulse being trapped in the photon sphere of the BH that forms in early stages of the evolution, and contributes to the global maximum. The global peaks of these series of evolutions follow an empirical law calculated as $\max K_1/A = \alpha\,(r_0/\sigma)^\gamma$, for small σ, where $\alpha = 33 \pm 3$ and $\gamma = 0.6 \pm 0.1$.

For a very crude estimate of what this means, arrange all neutrons in a neutron star in a shell of thickness σ close to the star radius, so as to maximize (23). Now let the configuration collapse, and find

$$\frac{\max K_1}{A} \lesssim 10^{13} \left(\frac{r_0}{10^4\,\mathrm{m}}\right)^{0.6} \left(\frac{10^{-15}\,\mathrm{m}}{\sigma}\right)^{0.6} . \tag{24}$$

Even in such a highly idealized (and impossible, since the neutron star material could not possibly be arranged in such a shell) configuration, one is far below the 76 orders of magnitude necessary to reach Planckian curvatures.

Finally, we note that in those cases where we ran our event horizon finder, we found that it forms slightly earlier than the apparent horizon, and that it covers a portion of approximately 50% of the observed Kretschmann peaks in figure 3.

6. BH binary merger

As an independent scenario, we have also investigated the time evolution of the curvature scalars in the inspiral and merger of a BH binary. We expect the curvature dynamics to be most pronounced around merger and therefore select for our study the relatively short (about 2 orbits) non-spinning, equal-mass binary labeled R1 in table I of [37]: each BH has a bare mass $m = 0.483$ and they start at $x = \pm 3.257$ with tangential momentum $P_y = \pm 0.133$ resulting in a total BH mass of $M = 1.01$ (all in code units).

We simulate this binary with the Lean code [38] which is based on the Cactus computational toolkit [39] and employs Carpet [40] for mesh refinement. The Einstein equations are evolved using the Baumgarte–Shapiro–Shibata–Nakamura–Oohara–Kojima formalism [41–43] with the moving-puncture gauge [44, 45] and apparent horizons are computed with AHFinderDirect [46, 47].

In vacuum, the Riemann and Weyl tensor are identical and we compute the curvature scalars K_1 and K_2 from the electric and magnetic parts of the Weyl tensor

$$E_{\alpha\beta} = C_{\alpha\mu\beta\nu} n^\mu n^\nu \,, \quad B_{\alpha\beta} = \frac{1}{2} \epsilon_{\alpha\mu}{}^{\rho\sigma} C_{\rho\sigma\beta\nu} n^\mu n^\nu \,, \tag{25}$$

where n^μ denotes the timelike unit normal field; see [38, 48] for more details. In vacuum, equations (3) and (4) expressed in terms of the electric and magnetic parts become

$$K_1 = 8(E^{mn} E_{mn} - B^{mn} B_{mn}) \,, \tag{26}$$

$$K_2 = 16 E^{mn} B_{mn} \,, \tag{27}$$

where we have switched from (Greek) spacetime indices to (Latin) spatial indices since the electric and magnetic parts of the Weyl tensor are by construction purely spatial tensors, $E_{\mu\nu} n^\nu = 0 = B_{\mu\nu} n^\nu$.

Here, we are interested in the maximal values of the curvature scalars that are realized *outside* the BH horizons. This exclusion of the horizon's interior encounters three practical difficulties: (a) Failure to find an apparent horizon does not necessarily imply absence of a horizon. (b) Points outside the apparent horizon may be inside the event horizon. (c) For non-spherical horizons, it is technically challenging to determine if a given grid point is inside the horizon.

The first difficulty is mitigated by the high reliability of AHFinderDirect; in every simulation, the AH finder fails to determine a horizon at exactly one time step around merger; we ignore this time step in our analysis. The second difficulty can only be overcome by computing event horizons which, however, is a highly complicated task (see e.g. [49]) and which we leave for future studies. Finally, we address the third challenge by evaluating two estimates of the maximum curvature, one by excising from the calculation a sphere with the *maximal* horizon radius and a second by excising instead a sphere with the *minimal* horizon radius. Both these radii are readily provided by AHFinderDirect together with the centroid of the horizon. The former gives us a conservative lower estimate for the maximal curvature (since we may have

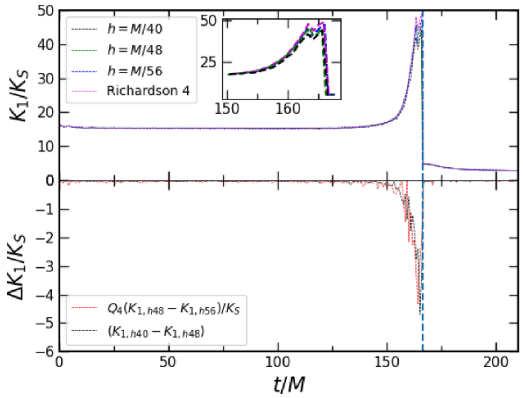

Figure 5. The curvature scalar K_1, maximized over space, is plotted as a function of time for a $\sim$2 orbit inspiral and merger of two non-spinning, equal-mass BHs. The upper panel shows the resulting $\max(K_1)$ for the three grid resolutions together with a fourth-order Richardson extrapolation. The bottom panel shows the differences between low and medium, as well as between medium and high resolution. The latter is scaled with a factor $Q_4 = 2.333$ expected for fourth-order convergence. The vertical dotted line around $t/M \approx 166.5$ marks the first occurrence of a common apparent horizon. All curvature estimates are normalized to the Schwarzschild value on the horizon, equation (22).

discarded legitimate points outside the exact horizon) while the latter gives us a strict upper limit (every point ignored in this calculation is definitely inside the apparent horizon and, thus, also inside the event horizon). In the following, we refer to these two methods as the $r_{\rm min}$ and $r_{\rm max}$ methods.

We calibrate the numerical accuracy of our calculations with a convergence analysis obtained from three simulations using a grid setup

$$\{(208, 128, 72, 24, 12, 6) \times (1.5, 0.75),\ h\}\ .$$

That is, we have two inner refinement levels, each consisting of two boxes of 'radius' 0.75 and 1.5 centered around either BH, and 6 outer levels of 'radius' 6, 12, 24, 72, 128 and 208 (all in units of total BH mass M) centered on the origin. The grid spacing is h on the innermost level and increases by a factor 2 on each level further out. In figure 5, we plot the resulting maximal curvature obtained for the $r_{\rm max}$ method in units of the Kretschmann scalar K_S on the horizon of a Schwarzschild BH of mass M, equation (22). In order to reduce high-frequency noise in the convergence analysis, we compare in the lower panel of the figure the differences between our finite-resolution results using a 10 point running average of the function $\max(K_1)$. This high-frequency noise arises from the lego sphere nature of the region we discard from the evaluation of K_1; as the BHs move across the domain, 'optimal' grid points can cross the horizon, resulting in a sudden drop or jump in $\max(K_1)$. The averaging procedure does not significantly affect the resulting convergence estimate, but greatly enhances the readability of the figure; note that only differences in $\max(K_1)$ have been averaged in figure 5, but not $\max(K_1)$ itself.

The bottom panel demonstrates convergence close to fourth order which we employ in the Richardson extrapolation displayed in the upper panel. Based on this extrapolation, we obtain a discretization error of 4 % around merger and below 1 % throughout inspiral and ringdown.

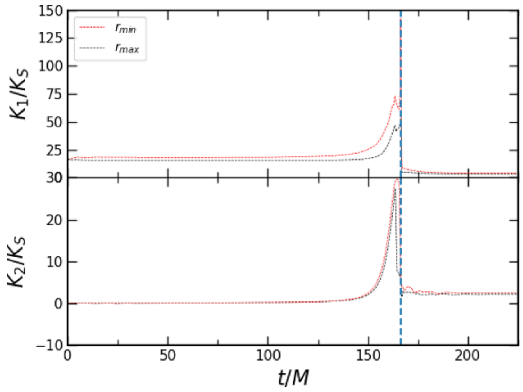

Figure 6. The curvature scalars K_1 and K_2, maximized in absolute value over space, are plotted as functions of time for a $\sim$2 orbit inspiral and merger of two non-spinning, equal-mass BHs. In each panel, the black curve shows the result obtained for the $r_{\rm max}$ method and the red curve shows the results for the $r_{\rm min}$ method. The vertical dotted line at $t/M \approx 166.5$ shows the time of first identification of a common apparent horizon.

The results for K_1 and K_2 extracted from our BH simulations are displayed in figure 6. For each scalar, we plot in this figure the maximum value obtained outside our $r_{\rm max}$ (black curves) and $r_{\rm min}$ (red curves) approximation of the apparent horizon. During the inspiral phase up to about $t = 150M$, we see that K_1 remains close to the value $K_1 = 16\,K_{\rm S}$ expected on the horizon of a Schwarzschild BH of mass $M/2$ while K_2 vanishes as expected for a non-spinning BH. Around merger, marked by the vertical dotted line in the figure, both curvature scalars rapidly increase to $K_1 \approx 75\,K_{\rm S}$ and $K_2 \approx 30\,K_{\rm S}$, respectively. In the upper panel we furthermore see a single spike where $K_1 \approx 150\,K_{\rm S}$. This spike, however, consists of a single data point, one time step before the first common horizon is found; we regard it as likely that this spike is spurious and may already be encompassed inside a common horizon which the code simply failed to compute. We have decided to still include this spike as a highly conservative upper limit for the maximal K_1 realized in our BH simulations.

After merger, the configuration rapidly settles down into a quiescent Kerr BH with mass $M_{\rm fin} = 0.965M$ and dimensionless spin $j_{\rm fin} = 0.688$. The curvature scalars correspondingly approach the late-time curvature extremals $K_1 = 2.95\,K_{\rm S}$ and $K_2 = 2.23\,K_{\rm S}$ for the $r_{\rm max}$ method. We can compare these values with the analytic expressions for the scalars of the Kerr BH spacetime which are given by equations (31) and (32) of [25],

$$K_1 = \frac{48M^2}{(r^2 + a^2\cos^2\theta)^6}\left(r^6 - 15r^4a^2\cos^2\theta + 15r^2a^4\cos^4\theta - a^6\cos^6\theta\right),$$

$$K_2 = \frac{96aM^2r\cos\theta}{(r^2 + a^2\cos^2\theta)^6}\left(3r^4 - 10r^2a^2\cos^2\theta + 3a^4\cos^4\theta\right), \tag{28}$$

where a is the Kerr parameter, i.e. $a = j_{\rm fin}M_{\rm fin}$ in our case. Maximized over the event horizon for a Kerr BH with the above mass and spin parameters, this gives us maximal curvature values $K_1 = 2.90\,K_{\rm S}$ and $K_2 = 2.43\,K_{\rm S}$ in good agreement with our numerical values.

In summary, the maximal visible curvature of the BH binary is close to that of the individual constituents during the inspiral and close to that of the Kerr remnant after merger. During the brief merger, maximal curvature values about one order of magnitude larger are realized, but clearly within a regime nowhere near where we would consider quantum aspects.

7. Conclusions

In this paper we considered a sequence of BH spacetimes of varying degrees of realism, computing the Kretschmann and Chern–Pontryagin scalars within each. Our focus was on the extent to which either could become larger than a stationary configuration characterized by a similar mass but, crucially, without permitting ourselves the freedom of fine-tuning towards large curvature. Starting with the collapse of dust, we found a moderate (25%) increase in the Kretschmann scalar when compared to the analogous Schwarzschild spacetime. In the collapse of null radiation we saw that whilst it is possible to build BH spacetimes with large curvature scalars in the domain of outer communication, such configurations require fine-tuning. Moving to the classic numerical example of the spherical collapse of a minimally coupled massless scalar field, we treated a number of sets of initial data. We found that the maximum value of the Kretschmann scalar in the BH exterior can, rather easily, be increased by factors of a few hundred relative to that at the horizon of a Schwarzschild BH with the same mass as the initial apparent horizon in the collapse. But increasing this value further appears to require fine-tuned initial data. To mitigate against the effect of fine-tuning in our plots, post-collapse, we renormalized by the maximum of the initial curvature scalar and the associated static BH mentioned above. Finally, we considered a binary BH spacetime. Once more, only a moderate increase of curvature scalars is seen in comparison to a reference Schwarzschild spacetime.

Overall, our results are very clear. They show that in four-dimensional spacetimes describing realistic collapse configurations or dynamical BH spacetimes, curvature never grows too large during the dynamics. In other words, without carefully tuning the initial data, it seems very difficult to dynamically enter in a regime that would not be described by the classical equations of motion. Classical remains classical.

Data availability statement

The data being used for the figures have been created using the methods analysed in the paper. Reproducing them should be straightforward. The data that support the findings of this study are available upon reasonable request from the authors.

Acknowledgment

V C is a Villum Investigator and a DNRF Chair, supported by VILLUM FONDEN (Grant No. 37766) and by the Danish Research Foundation under DNRF162. V C acknowledges financial support provided under the European Union's H2020 ERC Advanced Grant 'Black holes: gravitational engines of discovery' Grant Agreement No. Gravitas–101052587. Views and opinions expressed are, however, those of the author only and do not necessarily reflect those of the European Union or the European Research Council. Neither the European Union nor the granting authority can be held responsible for them. This project has received funding from the European Union's Horizon 2020 research and innovation programme under the Marie Sklodowska-Curie Grant Agreement No 101007855. We acknowledge financial support provided by FCT/Portugal through Grants 2022.01324.PTDC, PTDC/FIS-AST/7002/2020, UIDB/00099/2020 and UIDB/04459/2020. This work has been supported by STFC Research Grant No. ST/V005669/1 'Probing Fundamental Physics with Gravitational-Wave Observations'. This research project was conducted using computational resources at the Maryland Advanced Research Computing Center (MARCC). We acknowledge support by the DiRAC project ACTP284 from the Cambridge Service for Data Driven Discovery (CSD3)

system at the University of Cambridge and Cosma7 and 8 of Durham University through STFC capital Grant Nos. ST/P002307/1 and ST/R002452/1, and STFC operations Grant No. ST/R00689X/1. The authors acknowledge the Texas Advanced Computing Center (TACC) at The University of Texas at Austin and the San Diego Supercomputer Center for providing HPC resources that have contributed to the research results reported within this paper through NSF Grant No. PHY-090003. URLs: http://www.tacc.utexas.edu, https://www.sdsc.edu/.

ORCID iDs

Vitor Cardoso https://orcid.org/0000-0003-0553-0433
David Hilditch https://orcid.org/0000-0001-9960-5293
Krinio Marouda https://orcid.org/0000-0003-1030-8853
José Natário https://orcid.org/0000-0003-0885-9867
Ulrich Sperhake https://orcid.org/0000-0002-3134-7088

References

[1] Abbott B P *et al* (LIGO Scientific, Virgo) 2016 *Phys. Rev. Lett.* **116** 061102
[2] Abbott R *et al* (Scientific, Virgo) 2021 *Phys. Rev.* X **11** 021053
[3] Akiyama K *et al* (Event Horizon Telescope) 2019 *Astrophys. J. Lett.* **875** L1
[4] Abuter R *et al* (GRAVITY) 2020 *Astron. Astrophys.* **636** L5
[5] Berti E *et al* 2015 *Class. Quantum Grav.* **32** 243001
[6] Barack L *et al* 2019 *Class. Quantum Grav.* **36** 143001
[7] Berti E, Yagi K and Yunes N 2018 *Gen. Relativ. Gravit.* **50** 46
[8] Berti E, Yagi K, Yang H and Yunes N 2018 *Gen. Relativ. Gravit.* **50** 49
[9] Cardoso V and Pani P 2019 *Living Rev. Relativ.* **22** 4
[10] Bertone G and Tait T M P 2018 *Nature* **562** 51
[11] Brito R, Cardoso V and Pani P 2015 *Lect. Notes Phys.* **906** 1
[12] Penrose R 1965 *Phys. Rev. Lett.* **14** 57
[13] Penrose R 1969 *Riv. Nuovo Cim.* **1** 252
[14] Unruh W G and Wald R M 2017 *Rept. Prog. Phys.* **80** 092002
[15] Mathur S D 2005 *Fortschr. Phys.* **53** 793
[16] Giddings S B 2017 *J. High Energy Phys.* JHEP12(2017)047
[17] Birrell N D and Davies P C W 1984 *Quantum Fields in Curved Space* (*Cambridge Monographs on Mathematical Physics*) (Cambridge: Cambridge University Press)
[18] Parker L and Toms D 2008 *Quantum Field Theory in Curved Spacetime: Quantized Fields and Gravity* (*Cambridge Monographs on Mathematical Physics*) (Cambridge: Cambridge University Press)
[19] Burgess C P 2004 *Living Rev. Relativ.* **7** 5
[20] Endlich S, Gorbenko V, Huang J and Senatore L *J. High Energy Phys.* JHEP09(2017)122
[21] Agullo I, del Rio A and Navarro-Salas J 2017 *Phys. Rev. Lett.* **118** 111301
[22] del Rio A, Sanchis-Gual N, Mewes V, Agullo I, Font J A and Navarro-Salas J 2020 *Phys. Rev. Lett.* **124** 211301
[23] Cardoso V, Kimura M, Maselli A and Senatore L 2018 *Phys. Rev. Lett.* **121** 251105
[24] Emparan R 2020 *Int. J. Mod. Phys.* D **29** 2043021
[25] Cherubini C, Bini D, Capozziello S and Ruffini R 2002 *Int. J. Mod. Phys.* D **11** 827
[26] Natário J 2021 *An Introduction to Mathematical Relativity* (Berlin: Springer)
[27] Eardley D M and Smarr L 1979 *Phys. Rev.* D **19** 2239
[28] Christodoulou D 1984 *Commun. Math. Phys.* **93** 171
[29] Joshi P S and Malafarina D 2015 *Class. Quantum Grav.* **32** 145004
[30] Vaidya P C 1951 *Proc. Indian Acad. Sci.* A **33** 264
[31] Hiscock W A, Williams L G and Eardley D M 1982 *Phys. Rev.* D **26** 751
[32] Kuroda Y 1984 *Prog. Theor. Phys.* **72** 63

[33] Joshi P S 1997 *Global Aspects in Gravitation and Cosmology* (*International Series of Monographs on Physics*) (Oxford: Oxford University Press)
[34] Fayos F and Torres T 2010 *Class. Quantum Grav.* **27** 125011
[35] Bhattacharyya M K, Hilditch D, Nayak K R, Renkhoff S, Rüter H R and Brügmann B 2021 *Phys. Rev.* D **103** 064072
[36] Csizmadia P and Racz I 2010 *Class. Quantum Grav.* **27** 015001
[37] Baker J G, Centrella J, Choi D-I, Koppitz M and van Meter J 2006 *Phys. Rev.* D **73** 104002
[38] Sperhake U 2007 *Phys. Rev.* D **76** 104015
[39] Goodale T, Allen G, Lanfermann G, Massó J, Radke T, Seidel E and Shalf J 2003 *Vector and Parallel Processing - VECPAR' 2002, 5th Int. Conf. Lecture Notes in Computer Science* (Berlin: Springer)
[40] Schnetter E, Hawley S H and Hawke I 2004 *Class. Quantum Grav.* **21** 1465
[41] Nakamura T, Oohara K and Kojima Y 1987 *Prog. Theor. Phys. Suppl.* **90** 1
[42] Shibata M and Nakamura T 1995 *Phys. Rev.* D **52** 5428
[43] Baumgarte T W and Shapiro S L 1998 *Phys. Rev.* D **59** 024007
[44] Campanelli M, Lousto C O, Marronetti P and Zlochower Y 2006 *Phys. Rev. Lett.* **96** 111101
[45] Baker J G, Centrella J, Choi D-I, Koppitz M and van Meter J 2006 *Phys. Rev. Lett.* **96** 111102
[46] Thornburg J 1996 *Phys. Rev.* D **54** 4899
[47] Thornburg J 2004 *Class. Quantum Grav.* **21** 743
[48] Friedrich H 1996 *Class. Quantum Grav.* **13** 1451
[49] Diener P 2003 *Class. Quantum Grav.* **20** 4901